Electronic Supplementary Material (ESI) for ChemComm.
This journal is © The Royal Society of Chemistry 2018

A chemically-encoded timer for dual molecular delivery at tailored ranges and concentrations

Silvia Serra,[a] Ahmed Alouane,[b,c] Thomas Le Saux,[c] Steve Huvelle,[b,c] Raphaël Plasson,[d] Frédéric Schmidt,*[b] Ludovic Jullien*[c] and Raphaël Labruère*[a]

[a] Institut de Chimie Moléculaire et des Matériaux d'Orsay (ICMMO), CNRS, Univ Paris Sud, Université Paris-Saclay, 15 rue Georges Clemenceau, 91405 Orsay Cedex, France
[b] Institut Curie, PSL Research University Paris, CNRS UMR3666, INSERM U1143
26 rue d'Ulm, Paris, France
[c] PASTEUR, Département de chimie, École normale supérieure, PSL University, Sorbonne Université, CNRS, 75005 Paris, France
[d] Université d'Avignon - UFR-ip STS, UMR 408 Université d'Avignon – INRA, Campus Jean-Henri Fabre, 301 rue Baruch de Spinoza BP 21239, 84916 Avignon Cedex 9, France

The Supporting Information reports on:

- The synthesis of the caged compound **cS_2(C/DE)**;
- The photoconversion kinetic of **cS_2(C/DE)** upon UV illumination.

1. Synthesis of the caged compound cS_2(C/DE)

1.1 General

All chemical reagents were of analytical grade, obtained from Acros, Alfa Aesar, or Aldrich, and used without further purification. Solvents were obtained from Aldrich or VWR-Prolabo. Dichloromethane was dried on molecular sieves and used immediately. All reactions were performed under argon atmosphere, unless stated otherwise. Low actinic glassware was used for all experiments involving compounds bearing the nitroveratryl moiety. Analytical TLC was performed using Silica Gel 60 F254 pre-coated aluminum plates (Merck). Automated flash chromatography was performed on an Interchim Puriflash 430 system equipped with flash SIHP-JP silica cartridges. The following gradient of ethyl acetate in cyclohexane was used for elution: the elution started with an ethyl acetate/cyclohexane ratio of 3/97 for one column volume (CV); the ratio increased to 40/60 over 12 CV, kept for 2 CV, then increased to 100/0 over 2 CV, and finally kept at this value over 1 CV. The product detection was made by UV absorption at 254 nm. ^{1}H NMR spectra were recorded in $CDCl_3$ solution on a Bruker DRX 300 spectrometer at 300 MHz with tetramethylsilane (TMS) as internal standard. ^{13}C spectra were recorded on the same spectrometer in $CDCl_3$ solution at 75 MHz. Chemical shifts (δ) are expressed in ppm downfield from TMS. High-resolution mass spectrometry (HRMS) analyses were performed by electrospray with positive ionization (ESI+).

1.2 Experimental procedures

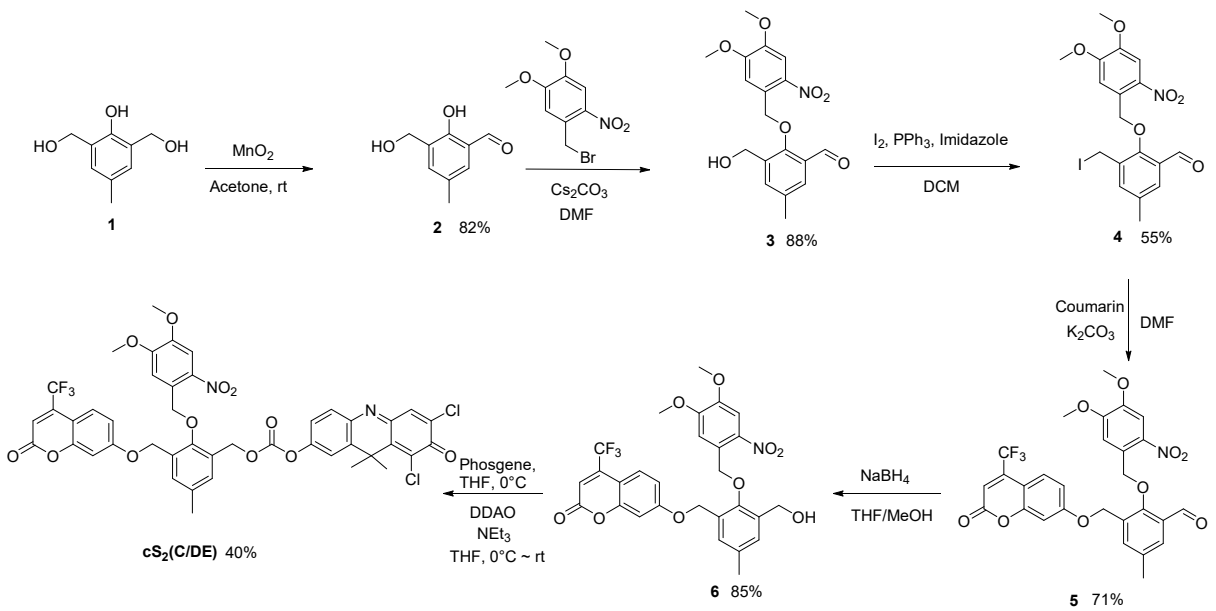

Scheme 1S. Synthetic pathway to **cS_2(DE/C)**.

2-Hydroxy-3-(hydroxymethyl)-5-methylbenzaldehyde (2). A mixture of 2,6-bis(hydroxymethyl)-*p*-cresol (12 mmol) and MnO_2 (92 mmol) in 250 ml of acetone was vigorously stirred at room temperature for 6 h, followed by filtration and washing with MeOH/acetone (3 × 30 ml). The crude

product was collected by evaporating the filtrate under reduced pressure and purified by automated flash chromatography to afford **2** as a white solid (82%). ^{1}H NMR (300 MHz, $CDCl_3$) δ 11.14 (s, 1H), 9.83 (s, 1H), 7.39 (s, 1H), 7.26 (s, 1H), 4.70 (s, 2H), 2.76 (s, 1H), 2.32 (s, 3H). ^{13}C NMR (75 MHz, $CDCl_3$) δ 196.7, 157.2, 136.9, 132.6, 129.1, 129, 120, 60.3, 20.3. HRMS-ESI(+): calcd for $C_9H_{10}NaO_3$ 189.0528, found 189.0521 $[M+Na]^+$.

2-((4,5-Dimethoxy-2-nitrobenzyl)oxy)-3-(hydroxymethyl)-5-methylbenzaldehyde (3). To a stirred solution of **2** (1.2 mmol) and 4,5-dimethoxy-2-nitrobenzyl bromide (1.2 mmol) in anhydrous DMF (10 mL) was added Cs_2CO_3 (2.4 mmol). The resulting mixture was stirred at room temperature for 3 h and CH_2Cl_2 (10 mL) and water (10 mL) were added. The organic phase was separated, dried over $MgSO_4$, and evaporated under reduced pressure. The crude residue was purified by automated flash chromatography to afford **3** as a yellow solid (88%). ^{1}H NMR (300 MHz, $CDCl_3$) δ 10.24 (s, 1H), 7.96 (d, J = 7.2 Hz, 1H), 7.75 (s, 1H), 7.59 (d, J = 11.2 Hz, 2H), 5.41 (s, 2H), 4.73 (s, 2H), 4.01 (d, J = 17.4 Hz, 6H), 2.60 (s, 1H), 2.39 (s, 3H). ^{13}C NMR (75 MHz, $CDCl_3$) δ 154.8, 153.8, 148.3, 140.1, 131.6, 130.4, 127.6, 127.5, 125.9, 123, 110, 107.8, 85.8, 73.3, 60.9, 56.4, 56.4, 20.8. HRMS-ESI(+): calcd for $C_{18}H_{19}NNaO_7$ 384.1053, found 384.1052 $[M+Na]^+$.

2-((4,5-Dimethoxy-2-nitrobenzyl)oxy)-3-(iodomethyl)-5-methylbenzaldehyde (4). To a solution of PPh_3 (1.1 mmol), imidazole (1.1 mmol), and iodine (1.1 mmol) in anhydrous CH_2Cl_2 (15 mL) was added **3** (0.55 mmol) under stirring. The resulting mixture was stirred at room temperature for 5 h and filtered to remove the precipitate. A saturated aqueous solution of $Na_2S_2O_3$ (20 mL) and CH_2Cl_2 (20 mL) were successively added to the filtrate. The organic phase was separated, dried over $MgSO_4$, and evaporated under reduced pressure. The crude residue was purified by automated flash chromatography to afford **4** as a white solid (55%). ^{1}H NMR (300 MHz, $CDCl_3$) δ 10.26 (s, 1H), 7.82 (s, 1H), 7.74 (s, 1H), 7.65 (s, 1H), 7.51 (s, 1H), 5.55 (s, 2H), 4.43 (s, 2H), 4.12 (s, 3H), 4.02 (s, 3H), 2.40 (s, 3H). ^{13}C NMR (75 MHz, $CDCl_3$) δ 155.7, 154.5, 148.4, 138.7, 131.9, 131.9, 131, 127, 126.7, 121.1, 108.5, 108.3, 89.7, 80.3, 57.8, 56.5, 29.5, 20.7. HRMS-ESI(+): calcd for $C_{18}H_{18}INNaO_6$ 494.0071, found 494.0059 $[M+Na]^+$.

2-((4,5-Dimethoxy-2-nitrobenzyl)oxy)-5-methyl-3-(((2-oxo-4-(trifluoromethyl)-2*H*-chromen-7-yl)oxy)methyl)benzaldehyde (5). To a solution of **4** (0.21 mmol) in anhydrous DMF (7 mL) was added K_2CO_3 (0.42 mmol) and 7-Hydroxy-4-(trifluoro-methyl)-2*H*-chromen-2-one (0.42 mmol) under stirring. The mixture was stirred at room temperature for 4 h and then CH_2Cl_2 (10 mL) and water (10 mL) were added. The organic phase was separated, dried over $MgSO_4$, and evaporated under reduced pressure. The crude residue was purified by automated flash chromatography to afford **5** as a white solid (71%). ^{1}H NMR (300 MHz, $CDCl_3$) δ 10.29 (s, 1H), 7.76 – 7.71 (m, 1H), 7.71 – 7.67 (m, 1H), 7.62 – 7.53 (m, 1H), 7.50 – 7.42 (m, 3H), 6.88 (s, 1H), 6.61 (s, 1H), 5.45 (s, 2H), 5.15 (s, 2H), 3.95 (d, J = 12.0 Hz, 6H), 2.43 (s, 3H). ^{13}C NMR (75 MHz, $CDCl_3$) δ 163, 162.6, 160.1, 159.5, 156.2, 153.6, 148.3, 140.1, 132.6, 132.1, 131.9, 131.8, 131.1, 128.9, 128.7, 127.2, 127.1, 126.4, 113.9, 112.3, 110.3,

107.2, 106.2, 73, 65.6, 60.4, 56.3, 20.8. HRMS-ESI(+): calcd for $C_{28}H_{22}F_3NNaO_9$ 596.1138, found 596.1120 $[M+Na]^+$.

7-((2-((4,5-Dimethoxy-2-nitrobenzyl)oxy)-3-(hydroxymethyl)-5-methylbenzyl)oxy)-4-(trifluoromethyl)-2*H*-chromen-2-one (6). To a solution of **5** (0.19 mmol) in THF (2 mL), $NaBH_4$ (0.28 mmol) dissolved in MeOH (1 mL) was added. The solution was stirred at room temperature for 3 h and saturated aq. NH_4Cl solution (10 mL) was added. CH_2Cl_2 (10 mL) was then added and the organic phase was separated, dried over $MgSO_4$, and evaporated under reduced pressure. The crude residue was purified by automated flash chromatography to afford **6** as a white solid (85%). ^{1}H NMR (300 MHz, $CDCl_3$) δ 7.66 (s, 1H), 7.45 (s, 1H), 7.24 – 7.03 (m, 2H), 6.99 (s, 1H), 6.66 (s, 1H), 6.50 – 6.20 (m, 2H), 5.34 (d, *J* = 23.3 Hz, 2H), 5.05 (s, 1H), 4.93 (s, 2H), 4.74 (s, 1H), 4.13 – 4.03 (m, 1H), 3.79 – 3.74 (m, 6H), 2.37 – 2.25 (m, 3H). ^{13}C NMR (75 MHz, $CDCl_3$) δ 163.8, 162.1, 153.8, 152.1, 148.3, 144.3, 144.2, 132.2, 132.2, 132.1, 132, 131.6, 131.4, 128.7, 128.7, 128.5, 110.2, 107.9, 103.2, 89.4, 85.9, 80, 73.3, 65.5, 59.3, 56.4, 56.4, 20.8. HRMS-ESI(+): calcd for $C_{28}H_{24}F_3NNaO_9$ 598.1301, found 598.1324 $[M+Na]^+$.

6,8-Dichloro-9,9-dimethyl-7-oxo-7,9-dihydroacridin-2-yl 2-((4,5-dimethoxy-2-nitrobenzyl)oxy)-5-methyl-3-(((2-oxo-4-(trifluoromethyl)-2*H*-chromen-7-yl)oxy)methyl)benzyl carbonate (cS$_2$(C/DE)). To a solution of **6** (0.017 mmol) in anhydrous THF (3 mL) at 0°C was quickly added a 20% solution of phosgene in toluene (0.1 mmol) via a syringe. The mixture was stirred at room temperature for 2 h and Ar gas was then bubbled through the solution for 15 min to remove any unreacted phosgene. The purged solution was added dropwise to a solution of Et_3N (0.12 mmol) and DDAO (0.017 mmol), in anhydrous THF (2 mL) and the mixture was cooled to 0 °C and stirred for 1 h. The resulting suspension was diluted with CH_2Cl_2 (10 mL) and a 1 M HCl aqueous solution (10 mL) was added. The organic phase was separated, dried over $MgSO_4$, and evaporated under reduced pressure. The crude product was purified by automated flash chromatography to afford **cS$_2$(C/DE)** as a slightly colored solid (40%). ^{1}H NMR (300 MHz, $CDCl_3$) δ 7.72 – 7.51 (m, 5H), 7.38 (s, 2H), 7.30 (d, *J* = 2.3 Hz, 1H), 7.16 (d, *J* = 8.6 Hz, 1H), 6.91 (d, *J* = 6.7 Hz, 2H), 6.62 (s, 1H), 5.43 (s, 2H), 5.35 (s, 2H), 5.15 (s, 2H), 3.98 (s, 3H), 3.91 (s, 3H), 2.40 (s, 3H), 1.87 (s, 6H). ^{13}C NMR (75 MHz, $CDCl_3$) δ 173.2, 162.3, 162.1, 159.2, 159.1, 156.2, 154.1, 153.3, 152.7, 150, 147.9, 144.5, 140.2, 139.5, 139.4, 138.6, 137.5, 135.7, 135.3, 133, 132.8, 132.4, 129.1, 128.9, 128.1, 126.4, 123.5, 120.6, 119.1, 117.3, 113.9, 108.8, 107.9, 107.3, 101.7, 74.4, 66.1, 65.9, 56.6, 56.3, 29.7, 26.6, 22.7, 20.9. HRMS-ESI(+): calcd for $C_{44}H_{33}Cl_2F_3N_2NaO_{12}$ 931.1255, found 931.1287 $[M+Na]^+$.

2. Photoactivation of cS_2(DE/C)

2.1 Instruments

2.1.1 UV-Vis absorption

UV-Vis absorption spectra were recorded in 1 cm × 1 cm quartz cuvettes (Hellma) on a diode array UV-Vis spectrophotometer (Evolution array, Thermo Scientific) at 293 K. Molar absorption coefficients were extracted while checking the validity of the Beer-Lambert law.

2.1.2 Steady-state fluorescence emission

Corrected fluorescence spectra upon one-photon excitation were recorded at 293 K with a Photon Technology International QuantaMaster QM-1 spectrofluorimeter (PTI, Monmouth Junction, NJ). Solutions for fluorescence measurements were adjusted to concentrations such that the absorption maximum was around 0.15 at the excitation wavelength.

2.1.3 Irradiation experiments in cuvettes

Irradiations with a light-emitting diode (NCSU033B; Nichia Corp., Anan, Japan) filtered by ET360±40 nm (Chroma Technology, Bellows Falls, VT) were performed at 293 K upon continuously recording the fluorescence emission from 45 µL solutions in CH_3CN/0.1 M Britton-Robinson pH 8 buffer 1:1 (v:v) [1] contained in 0.3×0.5 cm^2 quartz fluorescence cuvettes (Hellma). The incident-light intensities were systematically calibrated by determining the kinetics of photoconversion of the α-(4-dimethylaminophenyl)-*N*-phenylnitrone into 3-(4-dimethylaminophenyl)-2-phenyloxaziridine in ethanol as described in reference [2]. Typical incident-light surfacic fluxes were within the 10^{-3} $Ein.m^{-2}.s^{-1}$ range.

2.1.4 Irradiation experiments under an epifluorescence microscope

For observation with fluorescence microscopy, the sample solution was placed between two glass coverslips separated by double sided adhesive tape (3M) and washed several times with ethanol and water. The resulting device was placed on a 1 mm thick copper slide in which a hole (10 mm diameter) had been drilled for observation with the microscope. This copper slide was mounted on an aluminum block thermostated at ±0.2°C by two thermoelectric coolers (CP 1.0-63-05L-RTV; Melcor, Trenton, NJ). The temperature was monitored using a TCS610 thermistor (Wavelength Electronics, Bozeman, MT), and feed-back loop was driven by a MPT10000 temperature controller (Wavelength Electronics).

Epifluorescence imaging of the sample was achieved on a home built microscope (Figure 1S). The setup incorporates three light sources. The 375 nm laser (16 mW, BCL016-375; Crystalaser, Reno, NV) was used to construct a light sheet from above the sample by means of three cylindrical lenses (LJ695RM, LJ1703RM, LJ629RM; Thorlabs, Newton, NJ). The light from two LEDs driven by LED1B power supply (Thorlabs) was used to image fluorescence emission. Blue (LXML-PB01, Lumileds, Amsterdam, Netherlands, filtered at 480±20 nm Semrock) and lime (LXML-PX01;

Lumileds, filtered at 580 ± 10 nm Chroma) LEDs were used to image fluorescence emission in the coumarin and DDAO emission channels respectively. Epifluorescence illumination was performed using a FF505-606-Di01 (Semrock, Rocherster, NY) dichroic mirror and a 10× objective (Fluar, NA 0.5; Zeiss, Jena, Germany). The collected emitted fluorescence was filtered by a bi-band filter (FF524-628; Semrock) and the final image was reconstructed on a CCD camera chip (Luca-R; Andor Technology, Belfast, Northern Ireland). All experiments were recorded at 2 Hz as 100 frames movies. One second after the start of the recording (2 frames), the shutter (SH05; Thorlabs) blocking the beam from the UV laser was opened during five seconds and then closed. The images displayed in the Main Text start at the first frame after closing the shutter to avoid interference of the illumination profile.

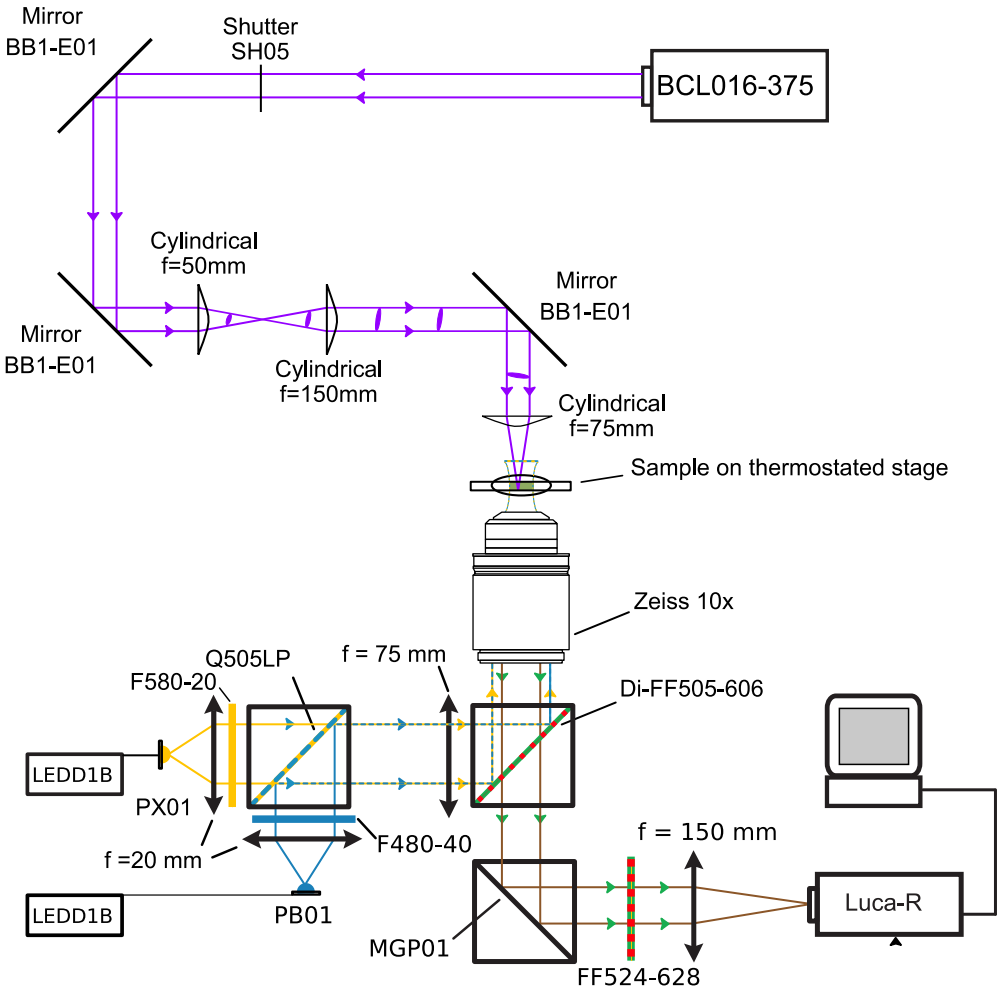

Figure 1S. Scheme of the epifluorescence microscope setup used for observation. See Text.

The illumination profile at 375 nm at the sample on the epifluorescence setup was obtained by imaging fluorescence emission after filling the sample holder with fluorescein disodium (1 µM in glycerol:water:acetonitrile 1:4:5). The power of the laser was measured with a Nova II powermeter (Ophir Optronics, Jerusalem, Israel) and the corresponding photon flux per unit of surface ($Ein.m^{-2}.s^{-1}$) was then extracted after measuring the illuminated surface at the sample plane. We found $I(375)(x) = I_0(375)\exp[-x^2/(2\,\sigma^2)]$ with I_0 = 13 mW and σ = 26 µm.

2.2 Kinetic analysis of self-immolation of the caged spacers

2.2.1 Theoretical model

The anticipated cascade of reactions leading to photo-release the fluorophores DDAO **D** and coumarin **C** from illuminating the caged precursor **cS$_2$(DE/C)** is shown in Scheme 2S.

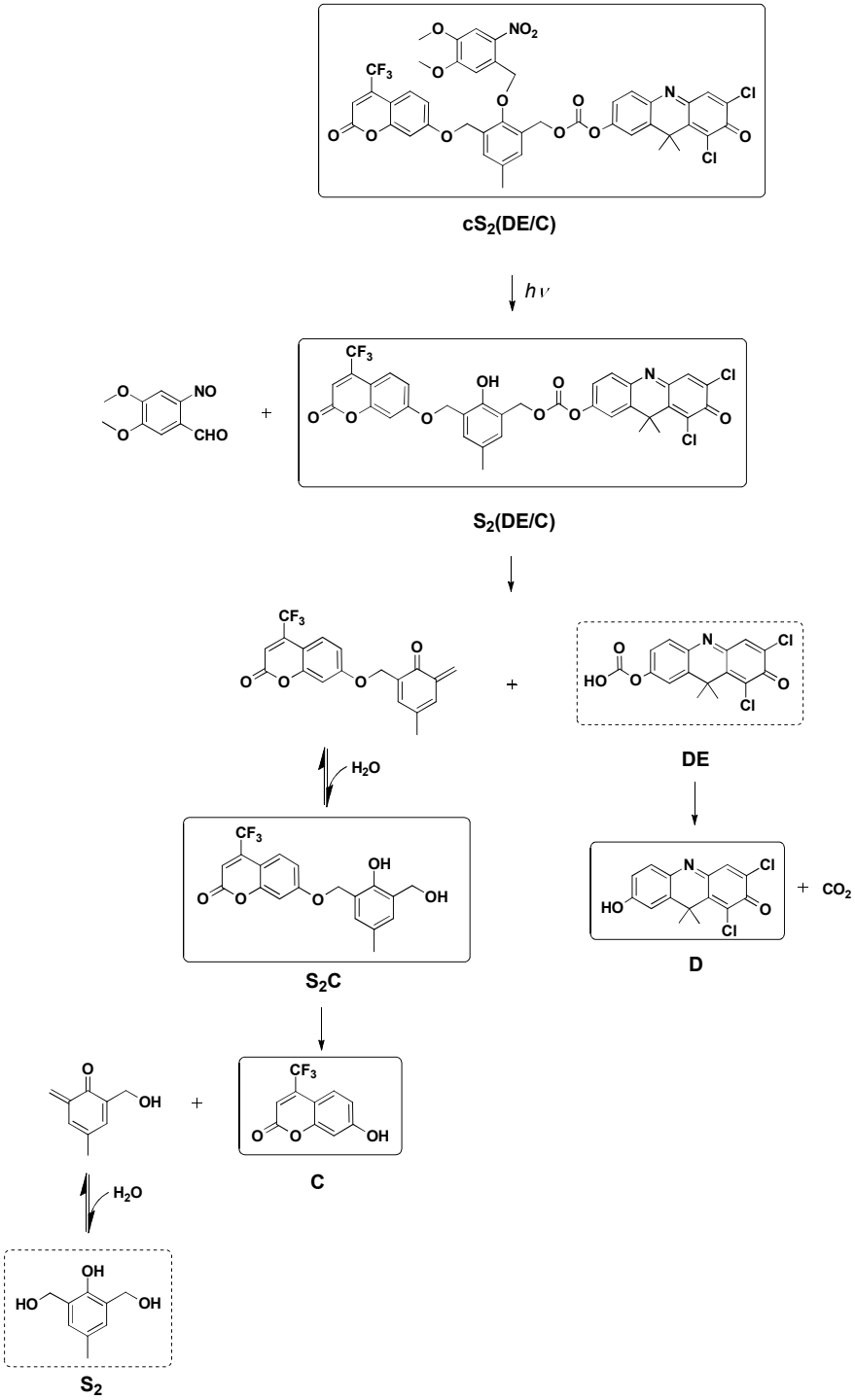

Scheme 2S. Reaction cascade expected to occur upon illuminating the caged spacer **cS$_2$(DE/C)**. The photochemical cleavage of the 4,5-dimethoxy-2-nitrobenzyl moiety initiates the self-immolation of the unstable

photo-released spacer **S_2(DE/C)**. The fast first quinone methide elimination leads to the formation of the DDAO-containing carbonic acid ester **DE** and the partially self-immolated-containing spacer **S_2C**. **DE** fast decomposition subsequently affords DDAO **D** together with carbon dioxide. Further self-immolation of **S_2C** yields **S_2** together with **C**. Note that the quinone methide intermediate is aromatized to the corresponding phenol in the presence of water.

To define the appropriate kinetic model for the cascade of reactions shown in Scheme 2S, we relied on our previous investigations [3-5]. Hence we first assumed that the carbonic acid DDAO ester **DE** would be released before the coumarin **C** due the carbonic linkage that attracts and accelerates the electronic delocalization in comparison to an ether bond. We also considered that the quinone methide eliminations were much slower than the subsequent carbonic acid ester decomposition. Thus we reduced the complete kinetic scheme to a model involving three successive reactions (associated to three rate constants: k_1, k_2, and k_3) leading to the formation of a product **P** from a reactant **R** via two intermediates **I_1** and **I_2** (Scheme 3S). Hence, the caged precursor **cS_2(DE/C)** (= **R**) first yields the phenol intermediate **S_2(DE/C)** (= **I_1**). **I_1** subsequently disassembles to provide the partially immolated spacer **S_2C** together with **D** and carbon dioxide (= **I_2**). **I_2** then affords the benzenic core **S_2** of the fully immolated spacer together with one molecule of **C** (= **P**). In the corresponding **RI_1I_2P** reduced scheme, the rate constant k_1 is associated to uncaging and would be correspondingly proportional to light intensity. In contrast, the rate constants k_2 and k_3 both refer to thermally-driven steps of quinone methide elimination.

$$\mathbf{R} \xrightarrow{k_1} \mathbf{I_1} \xrightarrow{k_2} \mathbf{I_2} \xrightarrow{k_3} \mathbf{P}$$

Scheme 3S. The **RI_1I_2P** kinetic model.

The set of differential equations governing the evolution of the concentration in the species shown in Scheme 3S is given in Eqs.(1-4):

$$\frac{dR}{dt} = -k_1 R \tag{1}$$

$$\frac{dI_1}{dt} = k_1 R - k_2 I_1 \tag{2}$$

$$\frac{dI_2}{dt} = k_2 I_1 - k_3 I_2 \tag{3}$$

$$\frac{dP}{dt} = k_3 I_2 \tag{4}$$

with the additional conservation law

$$R_0 = R + I_1 + I_2 + P \tag{5}$$

since the system is closed.

In the present case, the three rate constants k_1-k_3 are different and the solutions of Eqs.(1-4) are then given in Eqs.(6-9):

$$\frac{R(t)}{R_0} = e^{-k_1 t} \tag{6}$$

$$\frac{I_1(t)}{R_0} = \frac{k_1}{k_2 - k_1}\left(e^{-k_1 t} - e^{-k_2 t}\right) \tag{7}$$

$$\frac{I_2(t)}{R_0} = k_1 k_2 \left[\frac{e^{-k_1 t}}{(k_2-k_1)(k_3-k_1)} + \frac{e^{-k_2 t}}{(k_1-k_2)(k_3-k_2)} + \frac{e^{-k_3 t}}{(k_1-k_3)(k_2-k_3)}\right] \tag{8}$$

$$\frac{P(t)}{R_0} = 1 - \frac{k_2 k_3 e^{-k_1 t}}{(k_2-k_1)(k_3-k_1)} - \frac{k_1 k_3 e^{-k_2 t}}{(k_1-k_2)(k_3-k_2)} - \frac{k_1 k_2 e^{-k_3 t}}{(k_1-k_3)(k_2-k_3)} \tag{9}$$

The theoretical expressions of the temporal evolutions of the concentrations of the fluorophore-containing species would be correspondingly given in Eqs.(10-13):

$$cS_2(D/E)(t) = R(t) \tag{10}$$

$$S_2(D/E)(t) = I_1(t) \tag{11}$$

$$C(t) = P(t) \tag{12}$$

$$D(t) = k_1 k_2 \left[\frac{e^{-k_1 t}}{(k_2-k_1)(k_3-k_1)} + \frac{e^{-k_2 t}}{(k_1-k_2)(k_3-k_2)}\right] \tag{13}$$

2.2.2 Experimental results in cuvettes

Two series of illumination experiments have been performed. In the first series, we analyzed the DDAO photo-induced release. We correspondingly used light excitation at 365 nm (both for uncaging and exciting coumarin) and collected DDAO fluorescence emission at 660 nm for reporting. In the second series of illumination experiments, we analyzed the coumarin photo-induced release. We correspondingly used light excitation at 365 nm (both for uncaging and exciting coumarin) and collected coumarin fluorescence emission at 500 nm for reporting.

Figure 2a and d display the temporal evolution of the fluorescence signal $I_F^D(t)$ and $I_F^C(t)$ recorded with λ_{exc}=365 nm upon continuously illuminating the caged precursor **cS$_2$(DE/C)** at various light intensities at 365 nm at 293 K. The interpretation of these irradiation experiments requires to link the fluorescence signal to the concentrations in fluophore-containing components: **cS$_2$(DE/C)**, **S$_2$(DE/C)**, **S$_2$C**, **C**, **DE** and **D**. For a total absorbance lower than 0.15 (as in the present series of experiments), fluorescence emissions are proportional to the sum of the contributions of the fluorescent components, which are individually proportional to their respective concentrations

$$I_F^C(t) = \alpha^C\left[Q^C_{cS_2(DE/C)} cS_2(DE/C)(t) + Q^C_{S_2(DE/C)} S_2(DE/C)(t) + Q^C_{S_2C} S_2C(t) + Q^C_C C(t)\right] \tag{14}$$

$$I_F^D(t) = \alpha^D\left[Q^D_{cS_2(DE/C)} cS_2(DE/C)(t) + Q^D_{S_2(DE/C)} S_2(DE/C)(t) + Q^D_{DE} DE(t) + Q^D_D D(t)\right] \tag{15}$$

where $\alpha^{C,D}$ and $Q_i^{C,D}$ respectively designate a proportionality optical factor and the brightness of the species **i** under the illumination conditions used to record the signal in the channels associated to **C** and **D** emissions. Whereas absorption at 365 nm contains contributions from **cS$_2$(DE/C)**, **S$_2$(DE/C)**, **S$_2$C**, and **C**, the absorption at 645 nm is dominated by the **D** contribution. Hence upon illuminating **cS$_2$CD** at λ_{exc}=365 nm, we considered that only **cS$_2$(DE/C)**, **S$_2$(DE/C)** and **C** would contribute to the total fluorescence emission at λ_{em}=500 nm. In contrast, **D** only was expected to significantly contribute to fluorescence emission at λ_{em}=660 nm upon illuminating at λ_{exc}=365 nm. We additionally relied on our previous investigations [5] to neglect the brightness of **cS$_2$(DE/C)** and to admit that **S$_2$(DE/C)** and **DE** did not emit at 660 nm. We eventually wrote

$$k_1 = 2.3\varepsilon\varphi I_0 \tag{16}$$

which links the uncaging rate constant to the photochemical properties of the caging group (ε and φ respectively designate the molar absorption coefficient of the caging group and the quantum yield of the uncaging reaction) and to the surfacic light flux I_0.

We correspondingly ended up with the fitting laws (17,18)

$$I_F^D(t) = \alpha^D[Q_D^D D(t)] \tag{17}$$

$$I_F^C(t) = \alpha^C\left[Q^C_{S_2(DE/C)}S_2(DE/C)(t) + Q^C_{S_2C}S_2C(t) + Q^C_C C(t)\right] \tag{18}$$

to fit experimental data using $\alpha^{C,D}$, k_1, k_2, k_3, and the brightnesses as floating parameters.

2.2.3 Numerical simulations of the behavior observed in fluorescence microscopy

All numerical simulations were performed using the XMDS2 software [6]. The partial differential equation set (PDE) was based on the set of ordinary differential equations (1)-(4), with the addition of the chemical diffusion for all the compounds. The PDE set was solved for one dimensional systems in different geometries, using a standard adaptative Runge-Kutta of 4th/5th order.

A linear geometry was used, reproducing the irradiation of a two dimensional chemical system by a one-dimensional Gaussian light profile during five seconds. Integrations were performed using a discrete cosine transform, for implementing zero Neumann boundary conditions in a linear geometry, i.e. simulating a closed system. The profiles of the fluorescence emission have been considered to be proportional to the simulated concentration profiles. The numerical values of the rate constants measured in the cuvette experiments have been used as starting values. The diffusion coefficients were evaluated from the molecular geometries, using the Stokes-Einstein equation. Additional fine tuning of the numerical parameters was performed for fitting the experimental curves; hence k_2 was multiplied by 3, and the diffusion coefficients by 0.65. Best fit was eventually obtained for D_{cS2} = 1.6 10^{-10} m^2.s^{-1}, D_{S2} = 1.7 10^{-10} m^2.s^{-1}, D_{S2c} = 2.1 10^{-10} m^2.s^{-1}, D_C = 2.5 10^{-10} m^2.s^{-1}, D_D = 2.3 10^{-10} m^2.s^{-1}, D_S = 2.7 10^{-10} m^2.s^{-1}, k_1 = 4.7 s^{-1}, k_2= 1.1 10^{-1} s^{-1}, k_3=2.4 10^{-3} s^{-1}.

2.2.4 Observations in fluorescence microscopy

We imaged the temporal evolution of the fluorescence signals in the **C**- and **D**-emissive fluorescence channels after applying a one-dimensional Gaussian 375 nm light profile for 5 s on a 20 µM **cS_2(DE/C)** solution in 4.5/4.5/1 acetonitrile/Britton pH 8 buffer/glycerol (v/v/v) sandwiched between two glass plates. Figures 2Sa and b display the temporal evolution of the concentration profiles in the **D** emissive channel observed with fluorescence microscopy. In addition to Figures 2b and c, it further emphasizes on the excellent agreement between the experimental behavior and the numerical simulations.

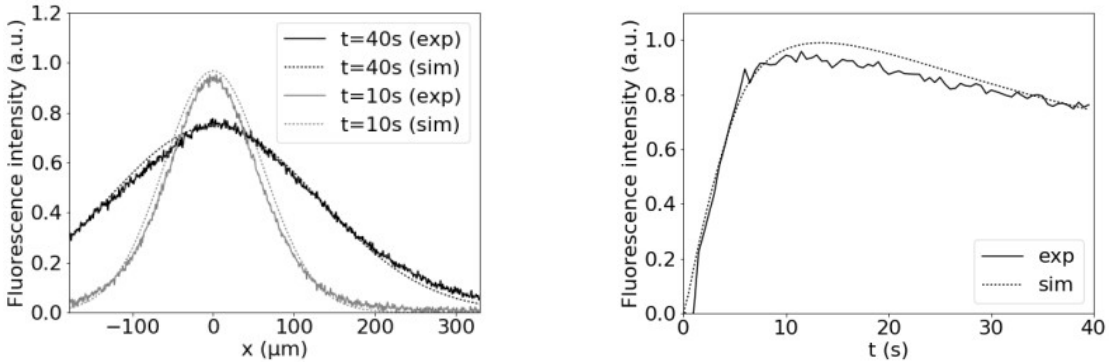

Figure 2S. Temporal evolution of the concentration profiles in the D emissive channel observed with fluorescence microscopy. Experimental and simulated fluorescence profiles (**a**) and their maximum (**b**) recorded in the D channel after 10 and 40 s. Solvent: 4.5/4.5/1 acetonitrile/Britton pH 8 buffer/glycerol (v/v/v); T = 293 K.

*2.2.3 Numerical simulations of liberation of **D** and **C** in spherical geometry at steady-state*

All numerical simulations were again performed using the XMDS2 software [6], and the set of ordinary differential equations (1)-(4) (with the addition of the chemical diffusion for all the compounds) which has been solved using a standard adaptative Runge-Kutta of $4^{th}/5^{th}$ order.

A spherical geometry was used, reproducing a constant irradiation within a sphere of radius $\mathcal{R}$ = 0.1 mm inside the system. Integrations were performed using a spherical Bessel transform, for implementing Dirichlet boundary conditions in a spherical geometry, i.e. simulating an open spherical system. For the sake of simplicity, all the diffusion coefficients were fixed to $\mathcal{D} = 10^{-9}$ $m^2.s^{-1}$, as a typical numerical values for diffusion in water, and the rate constants were taken in the $[10^{-7}\text{-}10^{2}]$ s^{-1} range. Starting from a uniform initial concentration in the **cS_2(DE/C)** precursor equal to c_0=1 mM, the system was taken as open to all compounds, and connected at its boundary to an infinite source of **cS_2(DE/C)** at concentration c_0 considered to be constant far from the activation locus.

In such a spherical geometry, one gets steady-state concentration profiles, which do not evolve in time. As anticipated from its fastest liberation, the steady-state concentration profile of **D** is more peaked and less extended than the one of **C** (Figures 3Sa and b). More precisely, with a precursor **cS_2(DE/C)** at c_0 = 1 mM concentration in the reservoir far from the activation site (here taken as a sphere of

R=100 μm diameter) and with precursors activations taking place at rate constants k_1 = 1 s^{-1}, k_2=10 s^{-1} and k_3=0.01 s^{-1}, the maximal concentrations of **D** and **C** are encountered at the activation locus with $[\mathbf{D}]_{max}/c_0$ = 0.11 and $[\mathbf{C}]_{max}/c_0$ = 0.66 with widths at half height equal to 117 and 526 μm for **D** and **C** respectively.

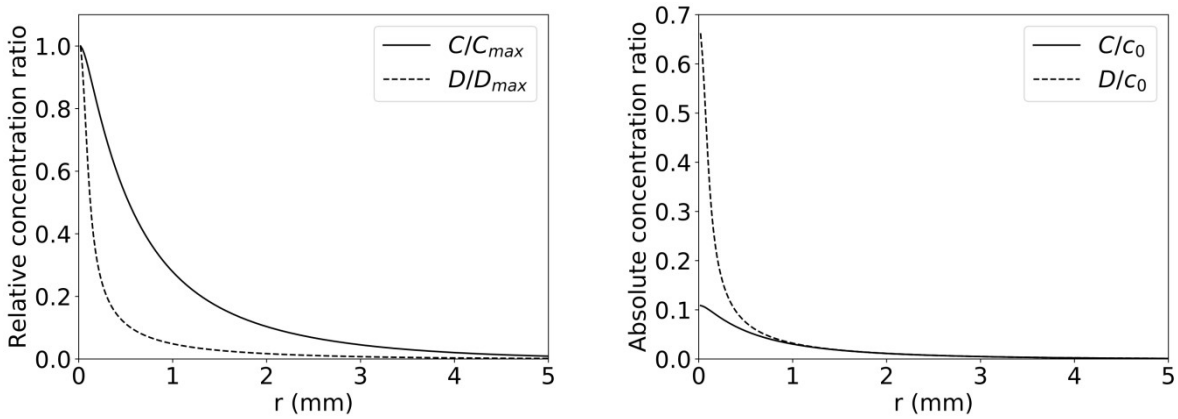

Figure 3S. *Stationary concentration profiles in **C** and **D** compounds for k_1=1 s^{-1}, k_2=10 s^{-1} and k_3=0.01 s^{-1}.* **a** corresponds to the concentration ratio C/C_{max} and D/D_{max}, C_{max} and D_{max} being the maximal concentrations in **C** and **D**, and **b** corresponds to the concentration ratio C/c_0 and D/c_0, c_o being the initial concentration in $\mathbf{cS_2}$.

3. Supplementary Information References

[1] C. Frugoni. Tampone universale di Britton e Robinson a forza ionica costante. *Gazz. Chim. Ital.* **1957**, *87*, 403-407.

[2] Wang, P. F. et al. Multichromophoric cyclodextrins. Antenna induced unimolecular photoreaction. Photo-isomerization of a nitrone. *New J. Chem.* **1996**, *20*, 895-907.

[3] Alouane, A. et al. Light-Activation for Versatile and Accurate Kinetic Analysis of Self-Immolative Spacers Disassembly. *Chem. Eur. J.* **2013**, *19*, 11717-11724.

[4] Alouane, A. et al. Self-Immolative Spacers: Kinetic Aspects, Structure–Property Relationships, and Applications. *Angew. Chem. Int. Ed.* **2015**, *54*, 7492-7509.

[5] Labruère et al. "Self-immolative" spacer for uncaging with fluorescence reporting. *Angew. Chem. Int. Ed.* **2012**, *124*, 9478-9481.

[6] Dennis et al. XMDS2: Fast, scalable simulation of coupled stochastic partial differential equations. *Comp. Phys. Chem*. **2013**, *184*, 201-208.